Raman Crystallographic Studies of the Intermediates Formed by Ser130Gly SHV, a β-Lactamase that Confers Resistance to Clinical Inhibitors†

Marion S. Helfand,*[,‡,§,||] Magdalena A. Taracila,[‡] Monica A. Totir,[⊥] Robert A. Bonomo,[‡,§,@] John D. Buynak,[#] Focco van den Akker,[||] and Paul R. Carey[||,⊥]

Research Service and Infectious Diseases Section, Louis Stokes Cleveland Department of Veterans Affairs Medical Center, and Departments of Medicine, Biochemistry, Chemistry, and Pharmacology, Case Western Reserve University, Cleveland, Ohio 44106, and Department of Chemistry, Southern Methodist University, Dallas, Texas 75275

Received March 26, 2007; Revised Manuscript Received May 14, 2007

ABSTRACT: Antibiotic resistance to β-lactam compounds in Gram-negative bacteria such as *Escherichia coli* and *Klebsiella pneumoniae* is often mediated by β-lactamase enzymes like TEM and SHV. Previously, a limited number of inhibitors have shown efficacy in combating such bacterial drug resistance. However, many Gram-negative pathogens have evolved inhibitor resistant forms of these hydrolytic enzymes. A single point mutation of the active site residue Ser130 to a Gly in either TEM or SHV results in resistance to amoxicillin and clavulanic acid, an important clinical β-lactam−β-lactamase inhibitor combination antibiotic. Previous structural and modeling studies of the S130G mutants of TEM and SHV have shown differences in how these two distinct but closely related enzymes compensate for the loss of the Ser130 residue. In the case of S130G SHV, a structure of tazobactam in the active site has suggested that the inhibitor preferentially assumes a *cis*-enamine intermediate form when the Ser130 hydroxyl is absent. Raman crystallographic studies of S130G SHV inhibited with tazobactam, sulbactam, clavulanic acid, and 2′-glutaroxy penem sulfone (SA2-13) were performed with the aim of identifying the type and amount of intermediate formed with each drug to understand the role of the S130G mutation in formation of the important enamine intermediates. It is demonstrated that with the exception of sulbactam, each compound forms observable *trans*-enamine intermediates. For S130G reacted with tazobactam, identical steady state levels of enamine are achieved when compared to those of wild-type (WT) or even deacylation deficient forms of the enzyme. With clavulanic acid, slightly smaller amounts of enamine are observed within the first 30 min of the reaction but are not significantly different than those for tazobactam. Thus, the resistance mutation does not substantially affect the amount of *trans*-enamine formed with clavulanic acid during the critical early time period of inhibition. This finding has important implications in the design of β-lactamase inhibitors for drug resistant variants like S130G SHV.

β-Lactam antibiotics such as penicillins, cephalosporins, and carbapenems are among the most widely used clinical therapeutic agents. Bacterial resistance in Gram-negative pathogens in the Enterobacteriaciae family, is evolving rapidly, especially when mediated by the presence of hydrolytic enzymes called β-lactamases. β-Lactamases perform their hydrolytic functions through one of two major mechanisms. One involves an activated serine hydroxyl functioning as a nucleophile; the other acts via a nucleophilic hydroxyl ion bound to one or two Zn^{2+} ions in the metallo-β-lactamase group (*1*). A widely used classification scheme based on sequence homology, the Ambler classification, designates the serine enzymes by groups A, C, and D, whereas the metalloenzymes are classified in group B (*2*). To date, hundreds of β-lactamase enzymes have been discovered in most species of bacteria (reviewed in refs *1* and *3*−*8*).

Clinical inhibitors of the class A enzymes of *Escherichia coli* and *Klebsiella pneumoniae*, the so-called TEM and SHV β-lactamases, respectively, were developed in the 1970s and 1980s to be given together with a β-lactam antibiotic (Figure 1). Typical combinations in use today include amoxicillin and clavulanic acid (Augmentin), piperacillin and tazobactam (Zosyn), and ampicillin and sulbactam (Unasyn). The inhibitors are themselves β-lactam compounds that interact with the active site Ser nucleophile at position 70 in the Ambler numbering scheme (*2*) and function as competitive, mechanism-based suicide inhibitors with typical affinities in the micromolar range. More recently, clinically significant

† M.S.H. is supported by a Department of Veterans Affairs Advanced Career Development Award. R.A.B. acknowledges the support of a Department of Veterans Affairs Merit Review Grant and NIH Grant R01 AI063517-01. P.R.C. is supported by NIH Grant R01 GM54072. F.v.d.A. is supported by NIH Grant AI062968, and J.D.B. is supported by the Robert A. Welch Foundation (Grant N-0871) and the Centers for Disease Control (Grant H75/CCH623342).

* To whom correspondence should be addressed: Research Division, Louis Stokes Cleveland Department of Veterans Affairs Medical Center, 10701 East Blvd., W151, Cleveland, OH 44106. Telephone: (216) 791-3800, ext. 4682. Fax: (216) 229-8509. E-mail: marion.helfand@case.edu.

‡ Louis Stokes Cleveland Department of Veterans Affairs Medical Center.

§ Department of Medicine, Case Western Reserve University.

|| Department of Biochemistry, Case Western Reserve University.

⊥ Department of Chemistry, Case Western Reserve University.

@ Department of Pharmacology, Case Western Reserve University.

Southern Methodist University.

10.1021/bi700581q CCC: $37.00
Published on Web 06/27/2007

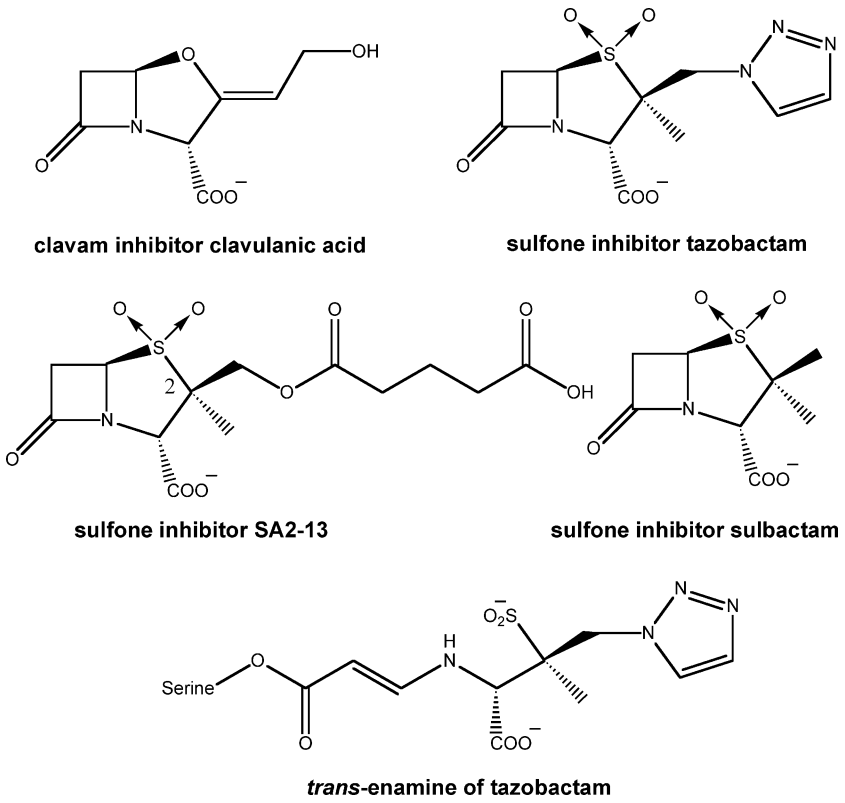

FIGURE 1: β-Lactamase inhibitors.

resistance to β-lactamase inhibitors, namely, against clavulanic acid, has been reported. Often, this resistance is due to the high-level expression of wild-type (WT)[1] TEM or SHV enzymes (*9*−*13*). However, TEM and SHV enzymes containing single point mutations that confer resistance to clavulanic acid also have been described. In the TEM family, clinical mutants containing M69I, -L, and -V, R244S, and S130G mutations have been reported (*10*, *13*−*19*). In SHV, clinical mutants containing the M69I and S130G mutations have been isolated (*20*, *21*). Typically, these inhibitor resistant mutants have been found in *E. coli* isolates causing urinary tract infections (*22*) which are often treated with the oral combination medication, amoxicillin and clavulanic acid. More recent surveys have found these organisms in respiratory secretions from surgical intensive care unit patients as well (*11*).

Numerous kinetic, modeling, and structural studies of the TEM and SHV S130G enzymes have been performed with the aim of understanding the structural basis of inhibitor resistance caused by this mutation (*23*−*25*). Previous studies of inactivation of S130G SHV β-lactamase using clavulanic acid and tazobactam have shown greater resistance toward clavulanic acid than toward tazobactam (*23*). Minimum inhibitory concentrations (MICs) for ampicillin and clavulanic acid are elevated but not for piperacillin and tazobactam. K_I values toward clavulanic acid are increased 332-fold compared to 60-fold for tazobactam when S130G SHV is compared to WT. Rates of inactivation are affected less dramatically (decreased 17 and 40% for clavulanic acid and tazobactam, respectively). Inactivation efficiency is decreased 420-fold for clavulanic acid and 100-fold for tazobactam, relative to that of WT. In timed inactivation experiments using clavulanic acid, after 20 min, S130G retains 50% of its activity compared to WT which is completely inhibited; tazobactam completely inhibits both enzymes on this time scale.

Because of the complex chemistry that takes place when an inhibitor binds to a β-lactamase enzyme (Scheme 1) and because of the role of Ser130 as a second nucleophile to initiate the final, irreversible step of inactivation [formation of the Ser130-bound vinyl carboxylic acid species (Scheme 1)], it was long assumed that loss of the Ser130 simply resulted in the loss of permanent inactivation of the enzyme causing inhibitor resistance. However, numerous studies have demonstrated the presence of a stable Ser70-bound species with both clavulanic acid and tazobactam (*26*, *27*). The 1.8 Å crystal structure of the S130G SHV tazobactam complex of Sun et al. (*24*) demonstrated that two-thirds of the enzyme active sites in the crystal were occupied by a *cis*-imine or enamine intermediate attached to Ser70. The remaining active sites contained a smaller, Ser70-bound, aldehyde fragment (Scheme 1). Molecular models and a crystal structure of the apoenzyme form of S130G SHV demonstrated that a critical active site water molecule had shifted from its usual position by 2 Å, due to loss of the Ser130 hydroxyl. In contrast, in the S130G TEM mutant apo structure (*25*), the active site

[1] Abbreviations: TEM, class A β-lactamase of *E. coli* first described in a Greek patient, with the name being derived from the patient's name; SHV, class A β-lactamase of *K. pneumoniae* initially thought to be a "sulfhydryl variant" of the TEM enzyme; SA2-13, 2′-glutaroxy penem sulfone, a novel class A β-lactamase inhibitor that preferentially stabilizes the *trans*-enamine; WT, wild type, in this context, referring to SHV-1 β-lactamase; MIC, minimum inhibitory concentration, a measurement used to determine whether bacteria are resistant or susceptible to specific antibiotics or antibiotic−inhibitor combinations; HEPES, *N*-(2-hydroxyethyl)piperazine-*N*′-2-ethanesulfonic acid; PBS, phosphate-buffered saline; HPLC, high-performance liquid chromatography; fwhm, full width at half-maximum; R^2, correlation coefficient.

Scheme 1: Tazobactam Inhibition Reaction with Class A β-Lactamase Enzyme

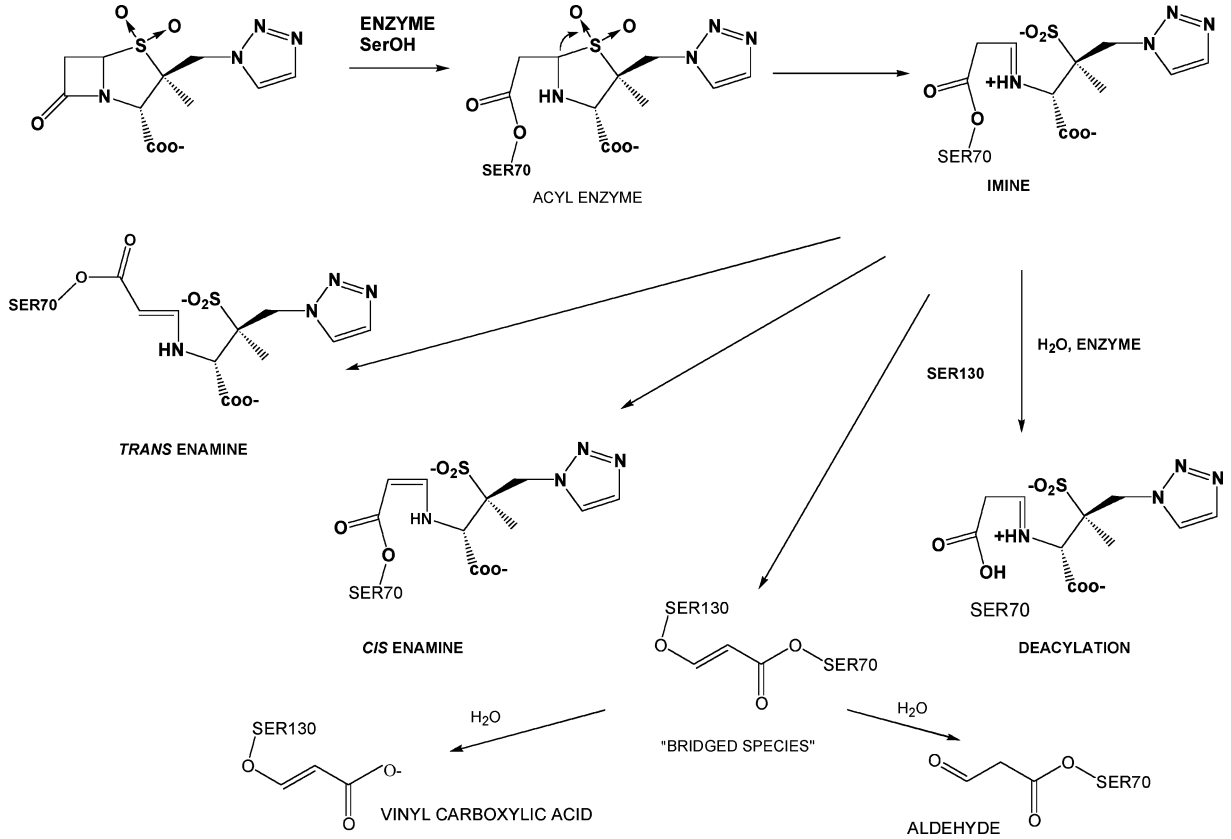

water was not displaced, and the Ser130 hydroxyl had been replaced by a second water molecule to account for this enzyme's retention of function.

We have applied Raman crystallography to study the interaction of β-lactam inhibitors with β-lactamase enzymes (*28*, *29*). Raman crystallography has many advantages. One is the ability to follow chemical reactions in single crystals in real time to provide guidance for X-ray crystallographic work (*29*−*31*). In addition, the nature of the intermediates, their relative populations, and their rates of formation and disappearance can be monitored in an attempt to learn more about the key steps in β-lactamase inhibition and the effect of enzyme mutations on the formation of these intermediates. Our previous Raman crystallographic studies of a deacylation deficient variant of SHV, E166A SHV (*28*), and a deacylation deficient variant with a known inhibitor resistance mutation, E166A/M69V SHV (*29*), demonstrated the importance of the *trans*-enamine intermediate of the clinical β-lactamase inhibitors. The M69V mutation was shown to influence the steady state population of *trans*-enamine with substantial reductions of observed enamine with both tazobactam and clavulanic acid in this model system. These studies led to the development of a new *trans*-enamine stabilizing compound, 2′-glutaroxy sulfone penem [SA2-13 (Figure 1)] whose 2′ linear charged side chain formed direct interactions with important class A active site residues such as Lys234, Ser130, and Thr235 (*32*).

To determine the effect of the S130G mutation on the population and type of enamine intermediates of the clinical inhibitors, we undertook Raman crystallographic studies to measure the type, amount, and rate of formation and disappearance of the enamine intermediates in single crystals of S130G SHV. As we will show through several lines of analysis, with tazobactam, the *trans*-enamine intermediate achieves the same steady state population in WT, E166A, and S130G SHV and is stable against deacylation for clinically significant periods in the S130G mutant. With clavulanic acid, S130G SHV takes slightly longer to achieve a steady state population of *trans*-enamine when compared to the reaction with tazobactam. However, the difference in these rates is not statistically significant, consistent with solution studies (*23*). Thus, the basis of clinical resistance to clavulanic acid seen with S130G SHV is not due to a reduced level of formation of the *trans*-enamine as previously reported for an M69V SHV variant (*29*).

EXPERIMENTAL PROCEDURES

Inhibitors. Li clavulanate (Glaxo-Smith-Kline), sodium sulbactam (Pfizer), and sodium tazobactam (Wyeth Pharmaceuticals) were kind gifts of industry. SA2-13 inhibitor was synthesized as described by Padayatti et al. (*32*). Fresh stock solutions (20−80 mM) in 2 mM HEPES buffer (pH 7.0) were prepared for use with the protein crystals. SA2-13 was suspended in phosphate-buffered saline (PBS, pH 7.4) at a stock concentration of 28 mM.

Protein Isolation and Purification. Ser130Gly SHV was generated by site-directed mutagenesis as previously described (*23*, *33*). Wild-type (WT) and Ser130Gly SHV proteins were expressed and purified using preparative isoelectric focusing and gel filtration HPLC (*23*, *34*).

Crystallization. β-Lactamase crystals were prepared in a modification of the method of Kuzin et al. (*28*, *35*). The same procedure was used to obtain both the wild-type and Ser130Gly SHV crystals.

Raman Crystallography and Spectral Analysis. Nonresonance Raman difference spectra of protein crystals and protein crystals soaked in inhibitor solutions were obtained as previously described (*28*). Raman spectra were collected using a Kaiser Optical Systems (Ann Arbor, MI) Raman microscope system and a Coherent Innova (Palo Alto, CA) 70C Kr ion laser at 647 nm and 120 mW laser power in a 20 μm spot size at the sample. The ambient temperature of the drop when the crystal is illuminated with 120 mW of laser power was 40 °C, measured using a thermocouple thermometer (Fisher Scientific). Data were analyzed using GRAMS/AI 7 (Thermogalactic, Inc., Salem, NH) as described previously (*28*). Difference spectra [protein + inhibitor − *F*(apoprotein)] were generated using subtraction factors, *F*, ranging from 0.7 to 1.1, to minimize the amide I band in the spectra. Because a more complex enamine band shape in the wild-type and S130G SHV Raman difference spectra was obtained, rather than using peak heights and normalizing to the peak height of the amide I band, a number of approaches to ascertaining the relative contribution of the enamine band to the Raman intensity in this region of the vibrational spectrum were taken. Prior data concerning the deacylation deficient E166A SHV with inhibitors were also reanalyzed by integrating the total peak area from 1606 to 1578 cm^{-1} and normalizing to the amide I area.

First, the total area of the peak in the S130G SHV−inhibitor enamine region was integrated, normalized to the total area of the amide I band in the spectrum, and plotted versus time (minutes) (Supporting Information). Alternatively, the peak area spanning 1606−1578 cm^{-1} was integrated, normalized to the amide I band area, and plotted versus time (Figure 3 and Supporting Information). Finally, the data were fitted using the peak finding algorithm in GRAMS/AI 7 (Thermogalactic, Inc.). Fits were performed in two ways. In one protocol, the program determined the number of frequency components under the entire S130G SHV−tazobactam difference spectrum enamine region band as well as the central frequencies of the bands, full widths at half-maximum (fwhm), peak heights, and shapes (mixture of Gaussian and Lorentzian line shapes); in the second procedure, the band shape was fitted with the number of frequency components and line shapes derived from the first procedure (typically two Gaussian components), where the first component was fixed at 1600 cm^{-1} with a fwhm of 10 cm^{-1} (from the phenylalanine band shape in the protein difference spectrum) with a variable peak height and the second component was fixed at 1593 ± 5 cm^{-1} [*trans*-enamine band center frequency ± spectral resolution obtained from the E166A tazobactam spectrum (Supporting Information)]. The intensity and fwhm of the enamine component were allowed to vary freely. The fitting algorithm utilized a least-squares method that converged after 50 iterations. R^2 correlation coefficients in these fits ranged from 0.8 to 0.99. The areas of the enamine component from the second fitting procedure were normalized to the amide I area and plotted versus time. Finally, the three methods of determining the amount of inhibition intermediate formed versus time were compared graphically to one another and also compared between the different SHV proteins and inhibitors (Supporting Information).

Ab Initio Calculations. Ab initio quantum mechanical calculations were performed to simulate the Raman frequencies of the *cis*- and *trans*-enamine intermediates of tazobactam, bound to a serine molecule using Gaussian 03 computational software (*36*). The structures of the serine-bound enamine intermediates were obtained by using the crystallographic coordinates from the S130G SHV−tazobactam structure (*24*) for the *cis* conformer and the E166A SHV−tazobactam structure (*30*) for the *trans* conformer. The calculations were performed using a Hartree Fock model chemistry with the 3-21G+* basis set with water solvation. Frequencies were corrected using a multiplicative factor of 0.9085 for this model chemistry (*37*).

RESULTS AND DISCUSSION

Raman Microscopy of a Deacylation Deficient Form of SHV β-Lactamase Demonstrates the Frequency, Band Shape, and Intensity of the trans-Enamine Species. As we have reported previously (*28*, *30*), the frequency, band shape, and intensity of the *trans*-enamine species of tazobactam at 100% occupancy in a SHV active site are obtained by measuring the Raman difference spectrum of E166A SHV crystals soaked in a 5 mM tazobactam solution for 20 min. This species is shown in Figure 2 (top trace), which shows a sharp single component band at 1592 cm^{-1} with a fwhm of 15 cm^{-1} and a normalized area of 150 000 ± 25 000 counts/cm. The base of this peak spans from 1606 to 1578 cm^{-1} and is used to estimate the area of the enamine signal in the wild-type and inhibitor resistant S130G SHV crystals.

The difference spectrum reveals that there is immediate loss of the carbonyl stretching frequency at 1780 cm^{-1} and the C−S stretch at 625 cm^{-1}, indicating breaking of the C−N bond in the β-lactam ring and the C−S bond in the thiazole ring upon acylation of the enzyme by the inhibitor (Figure 2, bottom trace, intact tazobactam). The triazole feature at 1293 cm^{-1} is retained and is an indicator of the amount of inhibitor soaked into the crystal. At higher concentrations of inhibitor in the drop surrounding the crystal, nonspecific binding can be observed as unhydrolyzed C═O or C−S resonances. Within 2−4 min of the reaction, a new peak is observed in each of the spectra, indicative of formation of an α,β unsaturated group previously identified as an enamine (*28*). In the case of E166A SHV as confirmed by the X-ray crystal structure of its complex with tazobactam (*30*), the sharp peak at 1592 cm^{-1} is due to the formation of the *trans*-enamine species (O═C−C═C−N−H) with >90% occupancy in the crystal.

The *trans*-enamine of clavulanic acid appears at 1610 cm^{-1}. In the deacylation deficient E166A enzyme, the maximal signal is observed at a concentration of 5 mM and a soaking time of 20 min, but there is less *trans*-enamine formed under these conditions than with tazobactam assuming 100% occupation of active sites and equal Raman scattering cross sections (*28*). Crystallographic studies required higher concentrations of clavulanic acid to achieve observable electron density in the X-ray studies (*31*), but at 50 mM, 100% occupancy was achieved.

The structure of the enamine portion of the clavulanate-derived intermediate is very similar to that of the tazobactam enamine, supporting the notion that the Raman scattering cross section from this part of the ligand should be similar. Some of the differences in the attainment of enamine populations noted previously with clavulanic acid in Raman

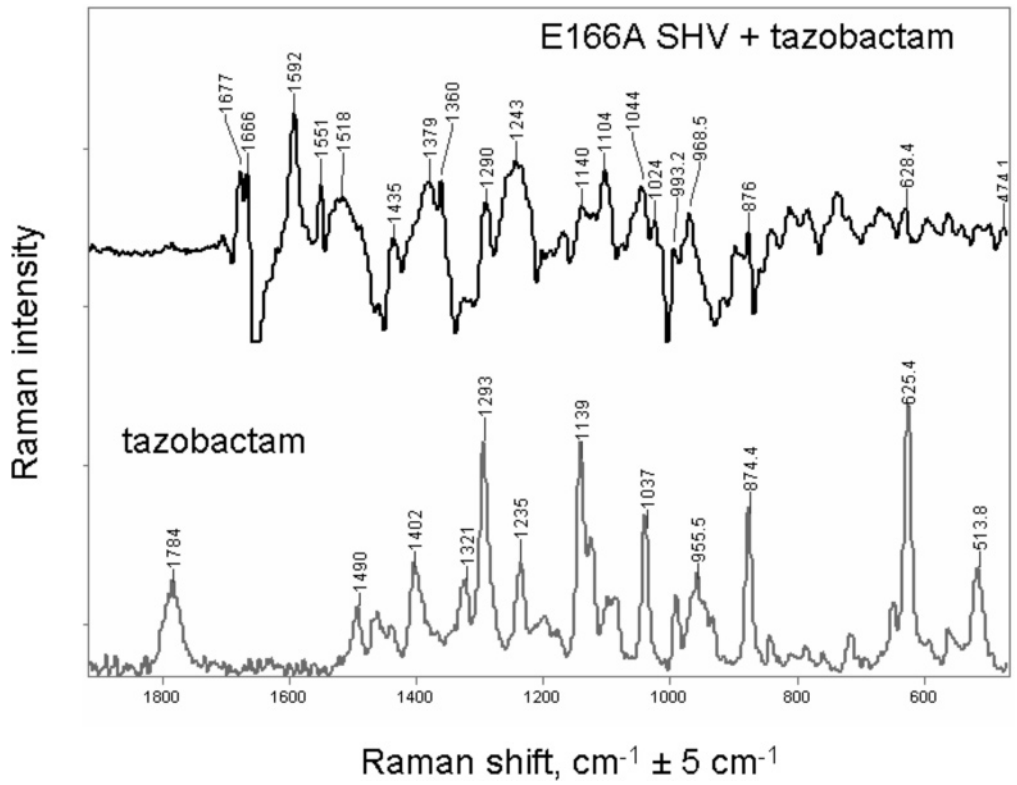

FIGURE 2: Raman difference spectra. The top trace (black) shows tazobactam bound to the E166A SHV deacylation deficient enzyme with the prominent appearance of the *trans*-enamine intermediate at 1592 cm^{-1}. The bottom trace (gray) shows the Raman difference spectrum of 20 mM tazobactam in 2 mM HEPES buffer (pH 7.0) with an intact carbonyl at 1784 cm^{-1}, a triazole at 1290 cm^{-1}, and a C−S thiazolium bond at 625 cm^{-1}.

and X-ray crystallographic work were attributed to the lack of stabilization of the tail end of the clavulanate enamine. For the purposes of the analysis that follows, steady state levels of an intermediate imply 100% occupancy only when enamine signals equal to those formed with tazobactam in E166A are observed. As we will show below, with complex, broad Raman band shapes, the use of normalized peak area to determine ligand populations is also preferred.

The Major Enamine Intermediates for Tazobactam Are Similar in S130G, E166A, and WT β-Lactamase. For tazobactam, Raman difference spectra, obtained after inhibition of WT, S130G, and E166A SHV for 30 min, are shown in Figure 3. In all three cases, there is an immediate decrease in the magnitude of the carbonyl stretching signal at 1783 cm^{-1} and the C−S stretch at ~625 cm^{-1} on acylation, and within 2−4 min of reaction, a new peak is observed in each of the spectra, indicative of formation of an enamine (*28*). For E166A as confirmed by the X-ray crystal structure of its complex with tazobactam, the sharp peak at 1591 cm^{-1} is due to the formation of the *trans*-enamine species with >90% occupancy in the crystal. The *trans*-enamine resonance for the WT SHV−tazobactam reaction is significantly broader but contains a component at 1594 cm^{-1}. The enamine resonance formed in S130G SHV is slightly broader (fwhm of 24 cm^{-1} vs 15 cm^{-1} in E166A SHV *trans*-enamine) but appears as a shoulder at ~1591 cm^{-1}, within the experimental error of the known *trans*-enamine frequency for tazobactam in the E166A SHV active site.

Following our studies of tazobactam inhibition of the E166A deacylation deficient variant of SHV, we obtained the structure of the observed Raman intermediates by allowing the Raman experiments to dictate the soaking in times and concentrations of inhibitors for crystallography (*28*, *30*) as described above. The crystal structure of tazobactam-inhibited WT SHV, obtained after soaking the crystal in 42 mM tazobactam for 96 h, has previously been shown to contain a *trans* species bound to Ser70 (assigned as imine or enamine), as well as an aldehyde form on Ser130 (*38*). An unreacted tazobactam molecule is observed to be bound nonspecifically near the opening of the active site. The Raman experiments with WT SHV inhibited with tazobactam, while not directly comparable to the Kuzin crystal structure (*38*), do suggest the presence of a transiently stabilized *trans*-enamine form at 1594 cm^{-1}. In addition, Raman crystal studies of SA2-13 with WT SHV show formation of a *trans*-enamine at a similar frequency (1590 cm^{-1}) and level of occupancy (*32*, *39*).

The crystal structure of S130G SHV with tazobactam (*24*) shows a *cis* form of the compound (assigned to enamine or imine). To compare the intermediates observed in the S130G crystal structures with our Raman studies of S130G SHV, the Raman reactions were allowed to proceed and were observed for 3 h, duplicating the experimental "soaking in" conditions of the crystallographers. We did alter the reaction conditions slightly by using 10 mM tazobactam in the surrounding drop (vs 20 mM in ref *24*), to minimize nonspecific binding. Despite the longer reaction time (3 h), we continued to observe a constant level of enamine in the crystal, without a shift in the band shape, frequency, or intensity, indicating that a steady state level of the 1591 cm^{-1} enamine inhibition intermediate had been achieved (data not shown). No additional resonances were observed to appear in the spectra. Similarly, when the Raman experiments were conducted using up to 80 mM tazobactam in the mother

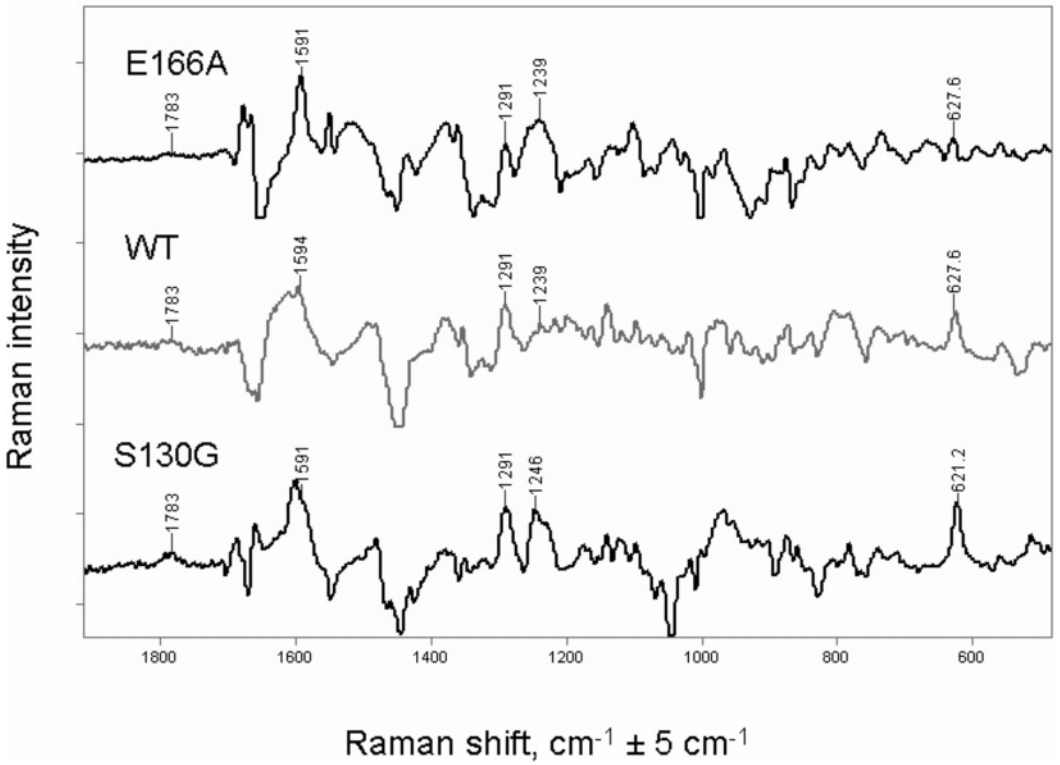

FIGURE 3: Non-resonance Raman difference spectra of E166A SHV (top), WT (middle), and S130G SHV (bottom) inhibited by tazobactam showing enamine at 1591−1594 cm^{-1} with a more complex band shape for WT and S130G SHV enzyme intermediates.

liquor drop, no changes in the appearance of the intermediate spectrum (data not shown) were observed other than an increase in the amount of unreacted tazobactam bound to the crystal.

The trans-Enamine Intermediate of 2′-Glutaroxy Penem Sulfone (SA2-13) in S130G SHV Appears at 1592 cm^{-1}. To confirm the assignment of the 1591 cm^{-1} band in the spectrum of tazobactam reacted with S130G SHV as the *trans*-enamine form, limited Raman experiments were conducted with the SA2-13 inhibitor (Figure 1). This inhibitor was designed to stabilize the *trans*-enamine intermediate in the SHV-1 active site and has been shown to form the *trans*-enamine in WT (*32*) and in S130G SHV (F. van den Akker, personal communication). The 2′-glutaroxy side chain forms a stabilizing salt bridge with Lys234 in the class A active site, as well as interactions with Ser130 and Thr235. The SHV−SA2-13 acyl enzyme complex is reactivated 10 times more slowly than the complex with tazobactam.

When ∼7 mM SA2-13 is soaked into crystals of S130G SHV and the reaction is followed with Raman crystallography, an enamine species is observed to appear at 1592 cm^{-1} with a fwhm of 12 cm^{-1}, consistent with the development of a *trans*-enamine species as previously observed (Supporting Information).

Ab Initio Calculations Reveal Differences in cis- and trans-Enamine Frequencies and Intensities. Previous analysis of the *cis*- and *trans*-enamine species frequencies and relative scattering cross sections by Hartree−Fock 6-311+g (d) ab initio calculations on simple model enamines showed that the *trans* and *cis* forms have different frequencies and that the *trans* form scattering cross section (relative intensity) is 3-fold higher than the *cis* form (*28*). Similar computations on the larger serine-bound enamine forms of tazobactam derived from crystal structures sufficiently show that the *cis* and *trans* frequencies are not equal, differing by 46 cm^{-1}. The *trans* intermediate has a >3-fold higher scattering cross section than the *cis* intermediate (Figure 4). In addition, the calculated spectrum for the *trans* intermediate better reproduces the qualitative features of the 1400−1200 cm^{-1} portion of the spectrum which reflects the triazole and carboxylate stretching motions of the ligand.

The trans-Enamine Intermediates for Tazobactam in S130G, E166A, and WT β-Lactamase Are Formed in Equal Amounts. Examination of the enamine band shape in the WT and S130G SHV−tazobactam spectra suggests that more than one frequency component is present (Figures 3 and 5). When the enamine band shape of the S130G SHV−tazobactam spectrum was analyzed using the peak finding algorithm of GRAMS/AI, two frequency components were detected, typically with one at ∼1600 cm^{-1} and one at ∼1595 cm^{-1}. The bands were Gaussian in shape with fwhm values of 10 and 40 cm^{-1}, respectively. These fits were consistent with the presence of a small peak from the protein phenylalanine at 1600 cm^{-1} and a "*trans*-like" enamine band. Allowing the program to use additional peaks to improve the fit had no effect on the number of components or their frequency, relative intensities, or fwhms. Fitting was also performed by restricting the band to contain two components, one fixed at 1600 cm^{-1} with a fwhm of 10 cm^{-1} (phenylalanine) and the other which was allowed to vary in width, intensity, and frequency by ±5 cm^{-1} around a central frequency of 1593 cm^{-1}. The two procedures gave similar results as far as the goodness of fit as determined by the R^2 correlation coefficient, and the amount and time dependence of the enamine species observed in the tazobactam-inhibited S130G SHV (Supporting Information). The amounts and time dependence determined this way also agreed with enamine versus time plots obtained by fitting the normalized area under the curve

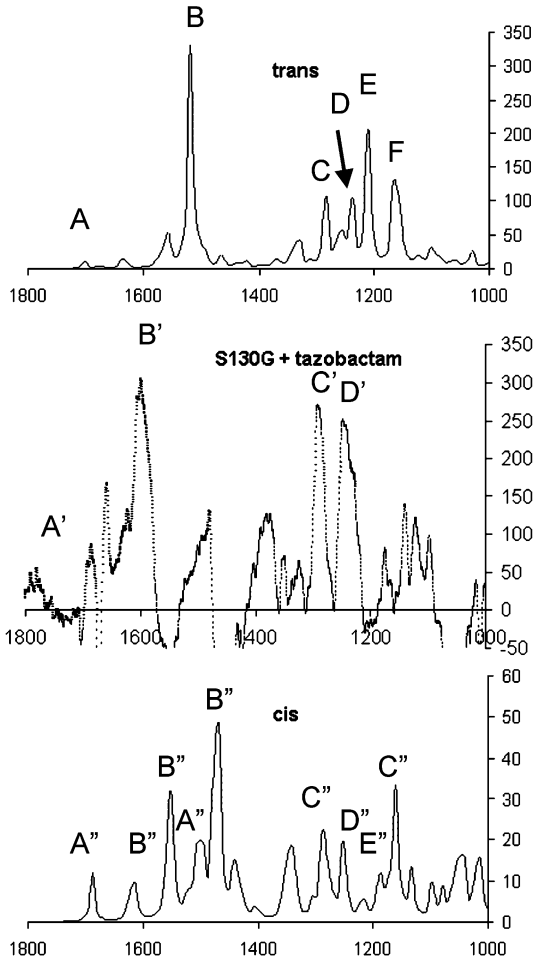

FIGURE 4: Gaussian simulations of the *trans*-enamine of tazobactam bound to serine and the *cis*-enamine of tazobactam bound to serine compared to the Raman experimental spectrum of S130G SHV with tazobactam. For the *trans* simulation (top): (A) 1702 and 1679 cm^{-1} for serine carboxylate and amino stretches, respectively, (B) 1633, 1576, and 1519 cm^{-1} for enamine (O═C−CH═CH−NH) bands with the major band at 1519 cm^{-1}, (C) 1284 cm^{-1} triazole and methylene stretches, (D) 1239 cm^{-1} enamine and C3 carboxylate stretch, (E) 1209 cm^{-1} enamine and methylene stretches, and (F) 1161 cm^{-1} triazole stretch. For the S130G SHV simulation with tazobactam: (A′) 1658 cm^{-1} subtraction of the amide I band, (B′) 1600 cm^{-1} Phe and 1591 cm^{-1} major enamine band, (C′) 1290 cm^{-1} triazole band, and (D′) 1243 cm^{-1} enamine band. For the *cis* simulation: (A″) 1688, 1626, and 1507 cm^{-1} serine carboxylate, amino, and Cα−H stretches, respectively, (B″) 1614, 1554, and 1465 cm^{-1} enamine stretches, where the major enamine band in *cis* is calculated at 1465 cm^{-1}, (C″) 1282 and 1160 cm^{-1} triazole stretches, (D″) 1249 cm^{-1} enamine and C3 carboxylate stretch, and (E″) 1185 cm^{-1} enamine and serine ester stretches. Note the lower intensity of the *cis*-enamine Raman spectrum and the shift to a lower frequency (1473 cm^{-1}) for the major band. The experimental data are scaled relative to the *trans* calculated intensities. The *trans* simulation reproduces the qualitative features of the major enamine band (1595 cm^{-1}) and the lower-frequency enamine and triazole (1400−1200 cm^{-1} region in the experimental spectrum).

from 1606 to 1578 cm^{-1} ("*trans*-enamine" region) (Supporting Information).

To prepare Figure 6, the normalized area under the curve in the *trans*-enamine region of the spectrum was plotted versus time. This demonstrates that the same amount of *trans*-enamine intermediate is formed for each enzyme with tazobactam, within the error of the measurements and the assumptions of the analysis. This is also consistent with the presence of only a *trans* species at 100% occupancy in the active site for both the WT and S130G SHV β-lactamases, since the *cis* species would have given a substantially weaker signal and would have appeared in a lower-frequency region of the spectrum.

The broader tazobactam *trans*-enamine bandwidth can be explained by the increased mobility of the linear *trans*-enamine inhibitor intermediate tail region, which is not stabilized by the water-mediated hydrogen bonding interaction between the triazole ring and Ser130 normally present (*29*). Band broadening is not seen with S130G SHV when it is inhibited by SA2-13 because this inhibitor forms a direct interaction between the 2′-glutaroxy side chain and Lys234 in the active site.

As a result of the frequencies and steady state populations attained for the enamine intermediates, the SA2-13 studies, and the *ab initio* calculations, we conclude that for tazobactam, the major enamine band in all three SHV enzymes, E166A, WT, and S130G, is a *trans*-enamine.

Steady State Levels of trans-Enamine Are Formed More Slowly in Inhibitor Resistant Ser130Gly β-Lactamase with Clavulanic Acid. The rates of formation and the amount of enamine intermediates formed are of interest, especially over time scales relevant to bacterial division in infectious disease (20−30 min). As is notable in Figure 6, the rates of formation and attainment of steady state levels of the enamine intermediates do not differ significantly for E166A, WT, and S130G SHV with tazobactam. The decay of the enamine intermediate is also similar for WT and S130G SHV. Even in S130G SHV, the tazobactam enamine intermediate achieves a stable, steady state level that persists out to at least 3 h after the inhibition reaction is initiated, and detectable enamine is present up to 48 h (data not shown). Decay of the enamine intermediate can occur due to reversion to the imine precursor, hydrolysis from the active site [least likely for *trans*-enamine due to multiple stabilizing interactions (*30*)], or progression further through the inhibition reaction to yield smaller irreversible products at either Ser70 or Ser130 (in the case of WT and E166A) (Scheme 1). The aldehyde form has not been detected in the Raman difference spectrum due to its presumably lower scattering cross section as compared to that of the enamine species. However, its presence in the active site as a Raman "dark" species would mean less than 100% occupancy by the enamine intermediate.

With clavulanic acid bound to S130G SHV (Figure 5), two features are seen in the enamine region of the spectrum, one at 1700 cm^{-1} which is due to the unsaturated hydrocarbon portion of the inhibitor and another feature at 1612 cm^{-1} corresponding to the enamine portion of the intermediate (*28*, *40*). The frequency and band shape of this enamine are identical to those found in E166A SHV, in which it has been verified by X-ray crystallography that the intermediate is in the *trans* conformation with a highly mobile tail region (*28*, *31*). The amount of enamine observed initially is slightly smaller than that found with tazobactam if scattering cross sections for the enamine portion of the molecule are assumed to be similar (Figure 7). However, the differences that are seen are within experimental error and thus are not likely to be significant.

Sulbactam forms little or no enamine intermediate with S130G SHV (data not shown) at the concentration used for tazobactam and clavulanic acid (10 mM). It requires ≫20

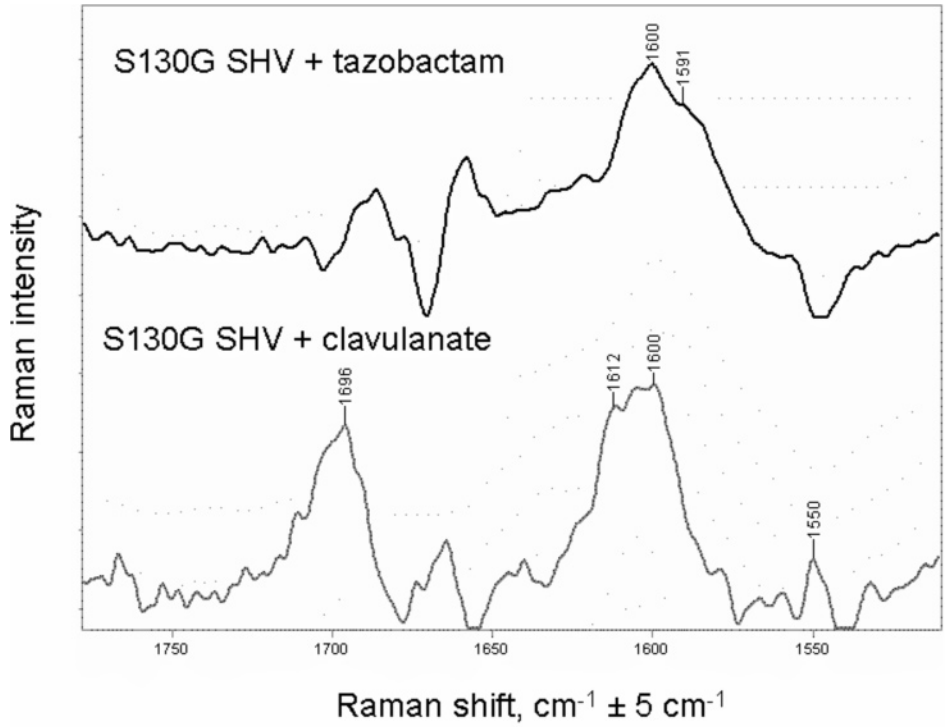

FIGURE 5: Spectra of S130G SHV with tazobactam and clavulanic acid and sulbactam after inhibition for 30 min showing the enamine band shapes (1591 cm^{-1} for tazobactam and 1612 cm^{-1} for clavulanic acid). Sulbactam forms little or no enamine intermediate at the concentration used with tazobactam and clavulanic acid (10 mM).

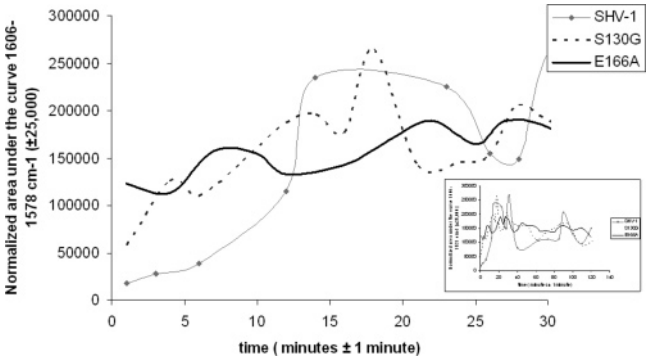

FIGURE 6: Time dependence of enamine formation with tazobactam in crystals of WT SHV-1 (gray trace with diamonds), S130G SHV (dashed trace), and deacylation deficient E166A SHV (solid trace). The signal intensity is normalized to the amount of enzyme by using the amide I band intensity in the Raman spectrum. S130G SHV forms amounts of enamine similar to those formed by E166A SHV and WT. The inset shows data for WT, S130G, and E166A SHV and tazobactam shown for a 2 h inhibition.

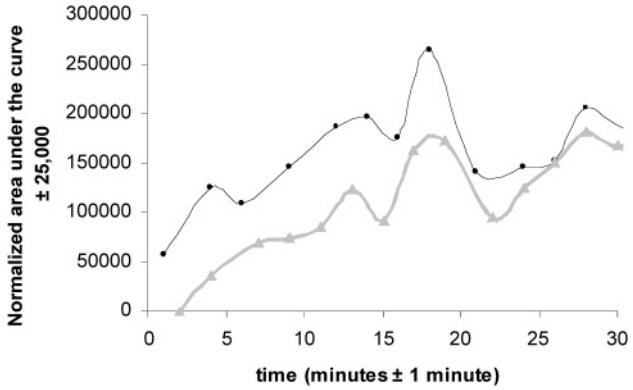

FIGURE 7: Early time dependence of enamine formation with tazobactam in crystals of S130G SHV (black) and S130G SHV with clavulanic acid (gray). The signal intensity is normalized to the amount of enzyme by using the amide I band intensity in the Raman spectrum. Steady state levels of enamine are formed somewhat more slowly with clavulanic acid than with tazobactam but are similar after 30 min.

mM for the observation of any detectable signal, indicating that the affinity of the Ser130Gly crystal for sulbactam is reduced or that the inhibitor is rapidly turned over so that a steady state level of intermediates is not achieved. Sulbactam generally has a higher turnover number toward class A enzymes, including SHV-1 and inhibitor resistant forms (*41*).

trans-Enamine Intermediates Are Stabilized in the Inhibitor Resistant S130G SHV β-Lactamase: The "Paradox" of Inhibitor Resistance Revisited. Previously, it has been noted that inhibitor resistance in S130G SHV is due mostly to its lowered affinity for clavulanic acid (0.14 μM vs 46.5 μM), which is less so for tazobactam (0.07 μM vs 4.2 μM) (*23*). However, rates of inactivation, once the Michaelis−Menten complex is formed, are similar to that of WT SHV (0.1 s^{-1} vs 0.06 s^{-1}, ±7%, for tazobactam; 0.03 s^{-1} vs 0.025 s^{-1} for clavulanic acid). In fact, turnover numbers (k_{cat}/k_{inact}) for these inhibitors were identical for the WT and S130G SHV enzymes [40 for clavulanic acid and 5 for tazobactam (*23*)]. This was termed the paradox of inhibitor resistance: despite loss of a key active site residue in formation of hydrolysis and inhibition intermediates and, perhaps more importantly, the resultant loss of a key active site water molecule (*23*, *24*, *27*), S130G SHV is fully capable of inhibition by mechanism-based inhibitors. Inhibitor resistance is the result of structural perturbations that disfavor formation of pre-acylation complexes, leading to reduced amounts of subsequent acyl enzyme intermediates and final products under conditions of limiting inhibitor concentration which are present in bacteria.

Our Raman crystallographic studies are conducted under conditions of sufficient inhibitor concentrations that achievement of minimal nonspecific binding and adequate signal-to-noise levels is possible. They are intended to demonstrate that enamines form in S130G SHV and to show their role, especially the *trans* intermediates, in the early (minutes to hours) phase of inhibition. Steady state levels of *trans*-enamines that reflect 100% occupancy of crystal active sites are achieved at similar rates with tazobactam, even for the inhibitor resistant variant, S130G SHV, with the same concentrations of inhibitor used for WT and E166A SHV. In general, the process of acyl enzyme formation and initial enamine formation is too rapid to be captured by the current Raman experimental configuration, so we are best able to characterize the steady state level of an intermediate in the protein crystals. In some cases [clavulanic acid with S130G SHV (Figure 7)], subtle differences in the rate of attaining steady state levels of *trans*-enamine formation may be apparent early in the reaction between the crystalline enzyme and the inhibitor, although under current experimental conditions with inhibitor concentrations of 10 mM, these are not significant.

The slower acylation rate due to the S130G mutation is likely offset by the fact that the active site water is also critical for deacylation, making the S130G enzyme relatively deacylation deficient like E166A SHV. Finally, the S130G residue is also required as the "second nucleophile", leading to formation of the bridged species and the vinyl carboxylic acid species. These pathways are unavailable for depletion of the *trans*-enamine population. Thus, even with clavulanic acid, observed steady state levels of the *trans*-enamine intermediate rapidly "catch up" to levels seen with E166A SHV.

These studies are in contrast to our previous studies with E166A/M69V SHV (*29*) in which the M69V mutation is not expected to affect deacylation or final product formation rates significantly when they are compared to those of the E166A variant. The M69V mutation affects the formation of the pre-acylation complex due to perturbation of the oxyanion hole (*29*), leading to smaller amounts of acyl-enzyme and *trans*-enamine. This perturbation may also affect acylation rates. Higher concentrations of inhibitor are required to achieve 100% occupancy of enamine species in the E166A/M69V SHV crystals with each of the clinical inhibitors (*29*), again reflecting an effect on inhibitor affinity and formation of the pre-acylation complex. Steady state levels of the *trans*-enamine in the M69V variant do not achieve levels seen with E166A SHV after 2 h with any of the inhibitors, indicating that either the intermediate deacylated more rapidly despite the presence of the E166A mutation or more likely acylation rates were severely affected.

The ability to stabilize *trans*-enamine intermediates has been emphasized in the design and structure−function analysis of the SA2-13 inhibitor (*32*). With the studies presented here, we have shown that the *trans*-enamine intermediates of tazobactam, SA2-13, and even clavulanic acid can be effectively stabilized in an inhibitor resistant enzyme like S130G SHV.

CONCLUSION

The evolution of drug resistance in class A β-lactamases has led to a variety of subtle and seemingly unique changes in the active sites of these enzymes. Numerous modeling, kinetic, and structural and spectroscopic studies of S130G SHV are yielding a clearer picture of how to overcome inhibitor resistance in bacteria expressing this β-lactamase enzyme.

Our Raman crystallographic studies have shown that enamine intermediates give rise to the same frequency in the deacylation deficient E166A, WT, and inhibitor resistant S130G SHV enzyme with tazobactam and clavulanic acid and achieve the same steady state populations at similar rates for these different enzymes. For WT and S130G SHV, reaction with the *trans*-enamine stabilizing inhibitor SA2-13 results in formation of a *trans*-enamine intermediate as determined by X-ray crystallography and Raman spectroscopy. Finally, *ab initio* quantum mechanical calculations predict that the *trans*- and *cis*-enamine intermediates of tazobactam derived from crystallographic structures will have very different enamine vibrational frequencies and Raman intensities. These findings support the assignment of the 1591 cm^{-1} band formed with tazobactam and the 1612 cm^{-1} band formed with clavulanic acid to the *trans*-enamine intermediate.

In S130G SHV, steady state levels of *trans*-enamine with clavulanic acid are achieved somewhat more slowly than with tazobactam over the first 30 min of reaction but are not different within experimental error. Thus, the reduced rate of *trans*-enamine formation does not account for the observed clinical resistance to this inhibitor. This indicates that C2-substituted inhibitors that form *trans*-enamines like tazobactam, clavulanic acid, and SA2-13 remain good lead compounds for the development of additional β-lactamase inhibitors that will overcome inhibitor resistance mutations. Modifications of clavulanic acid to improve affinity, increase acylation rates, or further stabilize its *trans*-enamine intermediate may enhance its ability to inhibit resistant class A β-lactamases.

ACKNOWLEDGMENT

We thank Christopher R. Bethel and Marianne P. Carey for assistance with initial expression and purification of the Ser130Gly SHV protein.

SUPPORTING INFORMATION AVAILABLE

A graphic demonstrating the band shape fitting procedure using the tazobactam-inhibited Ser130Gly enamine intermediate fitted with Phe 1600 cm^{-1} and enamine 1593 cm^{-1} components, a graph showing the steady state levels of the *trans*-enamine intermediate formed as determined by three different measurement procedures, and a Raman difference spectrum of S130G SHV β-lactamase with SA2-13 showing the formation of the *trans*-enamine intermediate at 1593 cm^{-1}. This material is available free of charge via the Internet at http://pubs.acs.org.

REFERENCES

1. Crowder, M. W., Spencer, J., and Vila, A. J. (2006) Metallo-β-lactamases: Novel weaponry for antibiotic resistance in bacteria, *Acc. Chem. Res. 39*, 721−728.
2. Ambler, R. P. (1980) The structure of β-lactamases, *Philos. Trans. R. Soc. London, Ser. B 289*, 321−331.
3. Babic, M., Hujer, A. M., and Bonomo, R. A. (2006) What's new in antibiotic resistance? Focus on β-lactamases, *Drug Resist. Updates 9*, 142−156.

4. Bush, K. (2001) New β-lactamases in Gram-negative bacteria: Diversity and impact on the selection of antimicrobial therapy, *Clin. Infect. Dis. 32*, 1085−1089.
5. Fisher, J. F., Meroueh, S. O., and Mobashery, S. (2005) Bacterial resistance to β-lactam antibiotics: Compelling opportunism, compelling opportunity, *Chem. Rev. 105*, 395−424.
6. Helfand, M. S., and Bonomo, R. A. (2003) β-Lactamases: A survey of protein diversity, *Curr. Drug Targets Infect. Disord. 3*, 9−23.
7. Jacoby, G. A., and Munoz-Price, L. S. (2005) The New β-Lactamases, *N. Engl. J. Med. 352*, 380−391.
8. Walsh, T. R., Toleman, M. A., Poirel, L., and Nordmann, P. (2005) Metallo-β-Lactamases: The Quiet before the Storm? *Clin. Microbiol. Rev. 18*, 306−325.
9. Gulay, Z., Bicmen, M., Amyes, S. G., and Yulug, N. (2000) β-Lactamase patterns and β-lactam/clavulanic acid resistance in *Escherichia coli* isolated from fecal samples from healthy volunteers, *J. Chemother. 12*, 208−215.
10. Leflon-Guibout, V., Speldooren, V., Heym, B., and Nicolas-Chanoine, M. (2000) Epidemiological survey of amoxicillin-clavulanate resistance and corresponding molecular mechanisms in *Escherichia coli* isolates in France: New genetic features of bla(TEM) genes, *Antimicrob. Agents Chemother. 44*, 2709−2714.
11. Perez-Moreno, M. O., Perez-Moreno, M., Carulla, M., Rubio, C., Jardi, A. M., and Zaragoza, J. (2004) Mechanisms of reduced susceptibility to amoxycillin-clavulanic acid in *Escherichia coli* strains from the health region of Tortosa (Catalonia, Spain), *Clin. Microbiol. Infect. 10*, 234−241.
12. Reguera, J. A., Baquero, F., Perez-Diaz, J. C., and Martinez, J. L. (1991) Factors determining resistance to β-lactam combined with β-lactamase inhibitors in *Escherichia coli*, *J. Antimicrob. Chemother. 27*, 569−575.
13. Stapleton, P., Wu, P. J., King, A., Shannon, K., French, G., and Phillips, I. (1995) Incidence and mechanisms of resistance to the combination of amoxicillin and clavulanic acid in *Escherichia coli*, *Antimicrob. Agents Chemother. 39*, 2478−2483.
14. Blazquez, J., Baquero, M.-R., Canton, R., Alos, I., and Baquero, F. (1993) Characterization of a new TEM-type β-lactamase resistant to clavulanate, sulbactam, and tazobactam in a clinical isolate of *Escherichia coli*, *Antimicrob. Agents Chemother. 37*, 2059−2063.
15. Zhou, X. Y., Bordon, F., Sirot, D., Kitzis, M.-D., and Gutmann, L. (1994) Emergence of clinical isolates of *Escherichia coli* producing TEM-1 derivatives or an OXA-1 β-lactamase conferring resistance to β-lactamase inhibitors, *Antimicrob. Agents Chemother. 38*, 1085−1089.
16. Henquell, C., Chanal, C., Sirot, D., Labia, R., and Sirot, J. (1995) Molecular characterization of nine different types of mutants among 107 inhibitor-resistant TEM β-lactamases from clinical isolates of *Escherichia coli*, *Antimicrob. Agents Chemother. 39*, 427−430.
17. Bermudes, H., Jude, F., Chaibi, E. B., Arpin, C., Bebear, C., Labia, R., and Quentin, C. (1999) Molecular characterization of TEM-59 (IRT-17), a novel inhibitor-resistant TEM-derived β-lactamase in a clinical isolate of *Klebsiella oxytoca*, *Antimicrob. Agents Chemother. 43*, 1657−1661.
18. Vedel, G., Belaaouaj, A., Gilly, L., Labia, R., Philippon, A., Névot, P., and Paul, G. (1992) Clinical isolates of *Escherichia coli* producing TRI β-lactamases: Novel TEM-enzymes conferring resistance to β-lactamase inhibitors, *J. Antimicrob. Chemother. 30*, 449−462.
19. Belaaouaj, A., Lapoumeroulie, C., Canica, M. M., Vedel, G., Névot, P., Krishnamoorthy, R., and Paul, G. (1994) Nucleotide sequences of the genes coding for the TEM-like β-lactamases IRT-1 and IRT-2 (formerly called TRI-1 and TRI-2), *FEMS Microbiol. Lett. 120*, 75−80.
20. Prinarakis, E. E., Miriagou, V., Tzelepi, E., Gazouli, M., and Tzouvelekis, L. S. (1997) Emergence of an inhibitor-resistant β-lactamase (SHV-10) derived from an SHV-5 variant, *Antimicrob. Agents Chemother. 41*, 838−840.
21. Dubois, V., Poirel, L., Arpin, C., Coulange, L., Bebear, C., Nordmann, P., and Quentin, C. (2004) SHV-49, a novel inhibitor-resistant β-lactamase in a clinical isolate of *Klebsiella pneumoniae*, *Antimicrob. Agents Chemother. 48*, 4466−4469.
22. Kaye, K. S., Gold, H. S., Schwaber, M. J., Venkataraman, L., Qi, Y., De Girolami, P. C., Samore, M. H., Anderson, G., Rasheed, J. K., and Tenover, F. C. (2004) Variety of β-lactamases produced by amoxicillin-clavulanate-resistant *Escherichia coli* isolated in the northeastern United States, *Antimicrob. Agents Chemother. 48*, 1520−1525.
23. Helfand, M. S., Bethel, C. R., Hujer, A. M., Hujer, K. M., Anderson, V. E., and Bonomo, R. A. (2003) Understanding resistance to β-lactams and β-lactamase inhibitors in the SHV β-lactamase: Lessons from the mutagenesis of SER-130, *J. Biol. Chem. 278*, 52724−52729.
24. Sun, T., Bethel, C. R., Bonomo, R. A., and Knox, J. R. (2004) Inhibitor-resistant class A β-lactamases: Consequences of the Ser130-to-Gly mutation seen in apo and tazobactam structures of the SHV-1 variant, *Biochemistry 43*, 14111−14117.
25. Thomas, V. L., Golemi-Kotra, D., Kim, C., Vakulenko, S. B., Mobashery, S., and Shoichet, B. K. (2005) Structural consequences of the inhibitor-resistant Ser130Gly substitution in TEM β-lactamase, *Biochemistry 44*, 9330−9338.
26. Sulton, D., Pagan-Rodriguez, D., Zhou, X., Liu, Y., Hujer, A. M., Bethel, C. R., Helfand, M. S., Thomson, J. M., Anderson, V. E., Buynak, J. D., Ng, L. M., and Bonomo, R. A. (2005) Clavulanic acid inactivation of SHV-1 and the inhibitor-resistant S130G SHV-1 β-lactamase. Insights into the mechanism of inhibition, *J. Biol. Chem. 280*, 35528−35536.
27. Pagan-Rodriguez, D., Zhou, X., Simmons, R., Bethel, C. R., Hujer, A. M., Helfand, M. S., Jin, Z., Guo, B., Anderson, V. E., Ng, L. M., and Bonomo, R. A. (2004) Tazobactam inactivation of SHV-1 and the inhibitor-resistant Ser130 → Gly SHV-1 β-lactamase: Insights into the mechanism of inhibition, *J. Biol. Chem. 279*, 19494−19501.
28. Helfand, M. S., Totir, M. A., Carey, M. P., Hujer, A. M., Bonomo, R. A., and Carey, P. R. (2003) Following the reactions of mechanism-based inhibitors with β-lactamase by Raman crystallography, *Biochemistry 42*, 13386−13392.
29. Totir, M. A., Padayatti, P. S., Helfand, M. S., Carey, M. P., Bonomo, R. A., Carey, P. R., and van den Akker, F. (2006) Effect of the inhibitor-resistant M69V substitution on the structures and populations of trans-enamine β-lactamase intermediates, *Biochemistry 45*, 11895−11904.
30. Padayatti, P. S., Helfand, M. S., Totir, M. A., Carey, M. P., Hujer, A. M., Carey, P. R., Bonomo, R. A., and van den Akker, F. (2004) Tazobactam forms a stoichiometric trans-enamine intermediate in the E166A variant of SHV-1 β-lactamase: 1.63 Å crystal structure, *Biochemistry 43*, 843−848.
31. Padayatti, P. S., Helfand, M. S., Totir, M. A., Carey, M. P., Carey, P. R., Bonomo, R. A., and van den Akker, F. (2005) High resolution crystal structures of the trans-enamine intermediates formed by sulbactam and clavulanic acid and E166A SHV β-lactamase, *J. Biol. Chem. 280*, 34900−34907.
32. Padayatti, P. S., Sheri, A., Totir, M. A., Helfand, M. S., Carey, M. P., Anderson, V. E., Carey, P. R., Bethel, C. R., Bonomo, R. A., Buynak, J. D., and van den Akker, F. (2006) Rational design of a β-lactamase inhibitor achieved via stabilization of the trans-enamine intermediate: 1.28 Å crystal structure of wt SHV-1 complex with a penam sulfone, *J. Am. Chem. Soc. 128*, 13235−13242.
33. Hujer, A. M., Hujer, K. M., and Bonomo, R. A. (2001) Mutagenesis of amino acid residues in the SHV-1 β-lactamase: The premier role of Gly238Ser in penicillin and cephalosporin resistance, *Biochim. Biophys. Acta 1547*, 37−50.
34. Helfand, M. S., Hujer, A. M., Sonnichsen, F. D., and Bonomo, R. A. (2002) Unexpected advanced generation cephalosporinase activity of the M69F variant of SHV β-lactamase, *J. Biol. Chem. 277*, 47719−47723.
35. Kuzin, A. P., Nukaga, M., Nukaga, Y., Hujer, A. M., Bonomo, R. A., and Knox, J. R. (1999) Structure of the SHV-1 β-lactamase, *Biochemistry 38*, 5720−5727.
36. Frisch, M. J., Trucks, G. W., Schlegel, H. B., Scuseria, G. E., Robb, M. A., Cheeseman, J. R., Montgomery, J. A., Jr., Vreven, T., Kudin, K. N., Burant, J. C., Millam, J. M., Iyengar, S. S., Tomasi, J., Barone, V., Mennucci, B., Cossi, M., Scalmani, G., Rega, N., Petersson, G. A., Nakatsuji, H., Hada, M., Ehara, M., Toyota, K., Fukuda, R., Hasegawa, J., Ishida, M., Nakajima, T., Honda, Y., Kitao, O., Nakai, H., Klene, M., Li, X., Knox, J. E., Hratchian, H. P., Cross, J. B., Bakken, V., Adamo, C., Jaramillo, J., Gomperts, R., Stratmann, R. E., Yazyev, O., Austin, A. J., Cammi, R., Pomelli, C., Ochterski, J. W., Ayala, P. Y., Morokuma, K., Voth, G. A., Salvador, P., Dannenberg, J. J., Zakrzewski, V. G., Dapprich, S., Daniels, A. D., Strain, M. C., Farkas, O., Malick, D. K., Rabuck, A. D., Raghavachari, K., Foresman, J. B., Ortiz, J. V., Cui, Q., Baboul, A. G., Clifford, S., Cioslowski, J., Stefanov, B. B., Liu, G., Liashenko, A., Piskorz, P., Komaromi, I., Martin,

R. L., Fox, D. J., Keith, T., Al-Laham, M. A., Peng, C. Y., Nanayakkara, A., Challacombe, M., Gill, P. M. W., Johnson, B. M., Chen, W., Wong, M. W., Gonzalez, C., and Pople, J. A. (2003) *Gaussian 03*, revision B.04, Gaussian, Inc., Pittsburgh, PA.

37. Foresman, J. B., and Frisch, E. (1996) Frequency Calculations: Predicting IR and Raman Spectra, in *Exploring Chemistry with Electronic Structure Methods*, p 64, Gaussian, Inc., Pittsburgh, PA.
38. Kuzin, A. P., Nukaga, M., Nukaga, Y., Hujer, A. M., Bonomo, R. A., and Knox, J. R. (2001) Inhibition of the SHV-1 β-lactamase by sulfones: Crystallographic observation of two reaction intermediates with tazobactam, *Biochemistry 40*, 1861−1866.
39. Totir, M. A. (2007) Raman Crystallographic Studies of Inhibitor Reactions in Class A and D β-Lactamases, Ph.D. Thesis, Case Western Reserve University, Cleveland.
40. Miani, A., Raugei, S., Carloni, P., and Helfand, M. S. (2007) Structure and Raman spectrum of Clavulanic Acid in Aqueous Solution, *J. Phys. Chem. B 111*, 2621−2630.
41. Thomson, J. M., Distler, A. M., and Bonomo, R. A. (2006) Interscience Conference on Antimicrobial Agents and Chemotherapeutics, San Francisco, CA.

BI700581Q